Zero-field NMR and NQR spectrometer

A. Bielecki, D. B. Zax,[a] K. W. Zilm,[b] and A. Pines

Department of Chemistry, University of California, Berkeley, and Materials and Molecular Research Division, Lawrence Berkeley Laboratory, Berkeley, California 94720

(Received 27 August 1985; accepted for publication 13 November 1985)

In comparison to high-field NMR, zero-field techniques offer advantages in terms of spectral interpretability in studies of polycrystalline or amorphous solids. This article describes a technique and apparatus for time-domain measurements of nuclear magnetism in the absence of applied fields (Fourier transform zero-field NMR and NQR). Magnetic field cycling and high field detection are employed to enhance sensitivity. The field cycling is accomplished with an air-driven shuttle system which moves the sample between regions of high and low magnetic field, in combination with switchable electromagnets in the low-field region. Sudden field steps or pulses are used to initiate coherent nuclear spin evolution in zero field and to monitor such evolution as a function of time. Experimental results are shown and analyzed. Possible variations on the basic method are described and their relative advantages are discussed.

INTRODUCTION

The interpretation of nuclear magnetic resonance (NMR) spectra of solids is made difficult by the dependence of the observed spectral frequencies on molecular orientation with respect to the applied magnetic field. In polycrystalline or amorphous solids, that orientational dependence in combination with the orientational disorder results in a spreading of spectral lines which commonly obscures most of the spectral information.[1] Matters are often improved by measuring the NMR spectrum in the absence of applied magnetic fields. Then the spectrum is characterized, for the most part, by splittings due exclusively to the "local" interactions, that is, interactions between the magnetic dipole moments of neighboring nuclear spins (dipolar interactions), or of nuclear electric quadrupole moments within the molecular-scale electric field gradients (quadrupolar interactions). With no external field defining a preferred spatial direction, the splittings due to these local nuclear interactions cannot depend on molecular orientation. Thus all equivalent molecules yield identical splittings independent of orientation and the spectral analysis is considerably simplified.

There is a problem, however, with observing NMR signals in zero field. The signal amplitude in any NMR measurement is proportional to the extent of spin ordering (e.g., magnetization), and usually proportional to the natural frequencies of the spin system. Since both of these factors increase with the field strength (when the Zeeman interaction is dominant, both are nearly proportional to the applied field), the application of a large magnetic field brings about an enormous gain in sensitivity. For this reason it is usually essential that measurements of nuclear magnetism be performed in high fields.

The dilemma presented here, that zero-field NMR offers higher resolution while high-field NMR offers higher sensitivity, can be resolved by "field cycling" techniques. In such schemes, fields are applied when needed to enhance sensitivity, and are removed for some other time to allow for probing the zero- (or low-) field behavior of the spin systems. Frequency-domain field cycling techniques, where the probing involves the application of a variable-frequency rf field, have been applied extensively to zero-field nuclear quadrupole resonance ("pure NQR") spectroscopy.[2–4] In time-domain techniques, the spin dynamics are instead probed as a function of a variable time interval; the resulting data may then be Fourier transformed to obtain spectra. Time-domain field cycling methods have until recently been used mostly for low-field NMR.[5] Field cycling is commonly applied to low-field nuclear relaxation studies[6]; such experiments can be conducted with time-domain measurements, although often this is not essential. The work presented here and other recent work[7] can be considered an extension of time-domain techniques to zero-field studies.

Figure 1 shows, in an idealized fashion, our field cycling scheme. The cycle consists of three periods which may be associated, respectively, with preparation, evolution, and detection. In the first period, a field is applied to magnetize the nuclear spins. This magnetization appears in a time on the order of the spin-lattice relaxation time, but the process of this relaxation is not shown explicitly. The field is suddenly switched to zero to initiate the second period, the evolution interval. In zero field, magnetization is not a stable form of spin order and it evolves at the natural frequencies of the spin system. To begin the final period, the field is suddenly switched back on, at which point the magnetization ceases to evolve and may be measured by high-field NMR techniques. The magnetization observed in a single field cycle corresponds to only a single value of the zero-field time. To determine how the magnetization varies as a function of time, the field cycle is repeated for regularly spaced values of the zero-field interval, and the evolution and decay of the magnetization is thus measured point by point. The Fourier transform of that magnetization function is equivalent to the zero-field absorption spectrum.

This article describes a practical technique and apparatus based on the idealized scheme above. It is presently the only generally applicable method for the observation of internuclear dipolar interactions in zero field. It can be used as

 0034-6748/86/030393-11$01.30

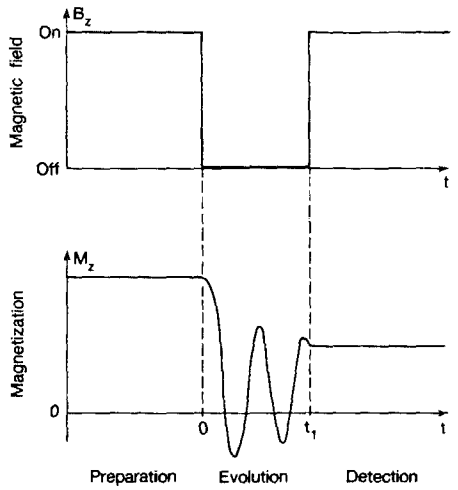

FIG. 1. At top, prototypical magnetic field cycle. At bottom, its effect on the bulk nuclear magnetization. During the preparation interval, magnetization is established consistent with equilibrium in the applied field. After the field is suddenly removed to begin the evolution interval, nuclear magnetization oscillates and decays under the influence of the local nuclear interactions. The field is suddenly reapplied to terminate evolution and to enable detection of the final magnetization by standard high-field NMR methods (for clarity, the detection pulse sequence is not explicitly shown here). By repeating the field cycle with zero-field intervals of various lengths and monitoring the resulting high-field magnetization signal, the zero-field magnetization decay can be detected point by point.

well for the observation of pure NQR signals when the natural frequencies are moderately low (this frequency limitation is determined by the practical characteristics of the apparatus). Thus it complements existing frequency-domain NQR methods, which as a rule perform best at higher frequencies.[2] Work is underway to develop new variations of the technique described here, which enhance the information content and the interpretability of the spectra.[8,9] The basic technique and apparatus given here can be adapted to such variant schemes, usually with little or no hardware modification.

I. THE TECHNIQUE

A. Field switching requirements

While the ideal field cycle shown in Fig. 1 features instantaneous field transitions, practical schemes require finite times to effect changes in the applied field. This causes no problem as long as the rapidity of the field switching meets two natural constraints. First, the field switching time τ_s should be short in comparison to the spin-lattice relaxation time T_1,

$$\tau_s \ll T_1 \qquad (1)$$

in order that the magnetization produced in high field not be lost during the field cycle. A second constraint governs the switching time when the instantaneous applied field is comparable in magnitude to the local fields (that is, when the Zeeman energy is comparable to the dipolar or quadrupolar energy). Then the switching time should be short relative to the natural periods (i.e., $1/\omega$) of the zero field evolution:

$$\tau_s \ll 1/\omega_{\max}\,, \qquad (2)$$

where $\omega_{\max}$ is the largest zero-field frequency of the spin system. If expression (2) is satisfied, the field shifts are sudden in the quantum mechanical sense. Field transitions less rapid than this bring about a partial disordering of the spins (or a transformation of spin order, e.g., adiabatic demagnetization) resulting in some loss and probable distortion of the observed zero-field signal. Since T_1 is always longer than $1/\omega_{\max}$, expression (1) is satisfied whenever expression (2) holds.

Field cycling experiments where the entire field transition is sudden, consistent with expression (2), are, in practice, not feasible. For most spin systems of interest, the zero-field evolution periods are on the order of microseconds or less. To obtain adequate sensitivity, the fields used for preparing and detecting the magnetization are necessarily large and uniform ($\gtrsim 10^4$ G, and relative inhomogeneity $\lesssim 10^{-5}$ over ~ 1 cm^3), and as such cannot be easily switched on or off in a matter of microseconds. However, it is generally unnecessary to carry out the entire field transition with such rapidity since expression (2) is important only when the applied field is within a limited range. It is therefore reasonable and more practical to execute each field transition in two steps, as illustrated in Fig. 2. In this scheme, the field is changed relatively slowly between the high field level and an intermediate field level, subject only to the first constraint of the spin-lattice relaxation time. Sudden field switching in keeping with the second constraint of quantum mechanical suddenness is attempted only between the intermediate field level and zero, where it is more feasible. As long as the intermediate field is somewhat larger than the local fields, the more practical field cycle of Fig. 2 and the simple one of Fig. 1 should affect the nuclear magnetism identically.

B. Selection of the intermediate field level

In the two-step cycle of Fig. 2, the size of the intermediate field is important because it determines the type of spin order which is to be prepared before and detected after the zero-field interval. When the Zeeman interaction in the intermediate field is at least comparable in magnitude to, and preferably larger than, the local interactions, the field cycle serves to prepare and then detect spin states which are approximately the eigenstates of the Zeeman Hamiltonian. Such states are generally nonstationary in zero field, and

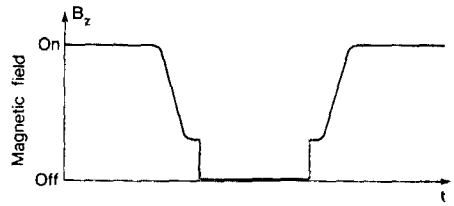

FIG. 2. Schematic representation of a practical field cycle. Since the preparation and detection fields must be large ($\gtrsim 10^4$ G), it is difficult to rapidly switch the entire field in one step as suggested by Fig. 1. The two-step field cycle shown here is technically more feasible. When the intermediate field level is larger than the local fields about the nuclei, the field cycles of Fig. 1 and this figure have identical effects on the nuclear spins.

their evolution gives information about the zero-field Hamiltonian. When the intermediate field is small compared to the local fields, the spin states which are prepared and subsequently detected tend to be more like the zero-field eigenstates. As a result, some fraction of the detected signal becomes nonevolving and results in a loss of useful signal, and an increase in the background signal. Moreover the signal loss is not generally uniform across the spectrum. Relative line intensities are affected, and analysis of the results becomes more difficult. It is desirable to avoid such problems by making the intermediate field at least several times as large as the local fields.

By equating the Zeeman frequency to the highest natural frequency of the spin system in zero field, and solving for the field, we obtain a useful definition of the marginal intermediate field, where the Zeeman and local interactions are of the same magnitude:

$$B_{\rm mar} = \omega_{\rm max}/\gamma\,, \tag{3}$$

where $B_{\rm mar}$ is the marginal intermediate field, $\omega_{\rm max}$ is the largest zero-field frequency, and γ is the gyromagnetic ratio of the nuclear species of interest. Where heteronuclear dipolar couplings are significant, the lowest of the values of γ should be used. Typical values of the marginal field range from about 10 G, for some dipolar coupled systems, to a few thousand gauss or more for nuclei with large quadrupolar interactions and small γ. In the apparatus to be described in Secs. I D and II, the intermediate field is nominally 100 G, which is generally appropriate for dipolar coupled spin systems. The apparatus can be adapted to other intermediate field levels, although when the required field is greater than about 1000 G, alternative methods[2] may prove more feasible.

C. Feasibility of rapid field switching

Sudden field switching appears to be most conveniently done by means of switchable electromagnets. The practical limitations on electromagnet switching often result from limitations of the power which can be transferred between the electrical power supply and the magnet. For an ideal electromagnet, the electrical power transferred while switching is simply the rate of change of magnetic energy with respect to time. For an approximate calculation, assume the intermediate field B is uniform over the sample volume V and zero elsewhere, and that the field transitions are exponential with time constant τ_s. Then the peak electrical power $P_{\rm peak}$ is

$$P_{\rm peak} = B^2 V/2\mu\tau_s \tag{4}$$

in rationalized MKS units and where μ is the magnetic permeability of the sample. When no ferromagnetic materials are present, $\mu \sim \mu_0$, the permeability of free space, and we shall assume this henceforth. Using expressions (2)–(4), an equation for the marginal power requirement is obtained in terms of the characteristics of the spin system:

$$P_{\rm peak} = \omega_{\rm max}^3\, V/2\mu_0\gamma^2\,. \tag{5}$$

For a typical quadrupolar coupled deuterium spin system with $\omega_{\rm max} = 2\pi\times 200$ kHz and $\gamma = 2\pi\times 654$ Hz/G, and a sample volume of 1 cm^3, this power amounts to about 470 W. The marginal field in this case is 310 G. The actual required power generally is greater than Eq. (5) indicates, since the switched field is not precisely uniform and localized about the sample as assumed above. Additionally one may opt to use intermediate fields and switching times better than marginal, in which case power requirements are much increased.

D. A practical technique

When the natural constraints imposed by the nuclear spins are considered along with the practicalities of magnets and of electronics, several reasonable methods of instrumentation can be devised. The method described in this section is one of the easier ways to adapt an ordinary pulsed NMR spectrometer to do zero-field NMR, but there are useful alternative methods, some of which are mentioned in Sec. V.

In our apparatus, the high-field portions of the experiment take place in a 42 kG persistent superconducting solenoid, with a room-temperature bore. For convenience, the superconducting solenoid is called the "main coil" in what follows. By means of a simple pneumatic shuttle system, the sample can be transported in a fraction ($\sim$0.15) of a second between the center of the main coil and a point outside, where the fringe field due to the main coil is 100 G. In that intermediate field region, the zero-field interval may be produced by applying a current pulse to an electromagnetic shielding coil which would be both rapidly switchable and capable of precisely canceling the fringe field in the region of the sample. For practical reasons, it is difficult to combine both functions in a single apparatus. Rather we use a set of two switchable electromagnet coils (in addition to the superconducting main coil) in the arrangement shown schematically in Fig. 3. In this scheme the characteristics of high speed and high precision are separated into two functionally independent magnet systems optimized for either characteristic separately. This considerably eases the design of the coils and of the associated switching electronics.

The coil labeled B_1 and its power source can be only slowly switched (in a few milliseconds) but are made to very accurately cancel the fringe field of the main coil B_0. In the 100-G fringe field, the B_1 coil (the "shielding coil") can consistently null the field to less than 100 mG. The coil B_2 (the "auxiliary coil") and its power source are not as accurate or well regulated, but instead are made to switch very rapidly. B_2 is used to apply an extra field during the switching transients of the coil B_1, and it provides the sudden field transitions needed for time-domain studies. In our apparatus, the field produced by B_2 is 100 ± 10 G. Its switching transitions are nearly exponential with a time constant of 300 ns.

The sequence used for going from the high field to zero field and back is illustrated in Figure 3 and described below: (1) The sample is moved from the main coil to the fringe field. During this period, both low-field coils are shut off. (2) Both coils are turned on. B_2 turns on quickly, maintaining an intermediate field at least as large as 100 G at the sample while B_1 is settling into its steady-state current. (3) After the current in B_1 settles, B_2 is turned off. Then the

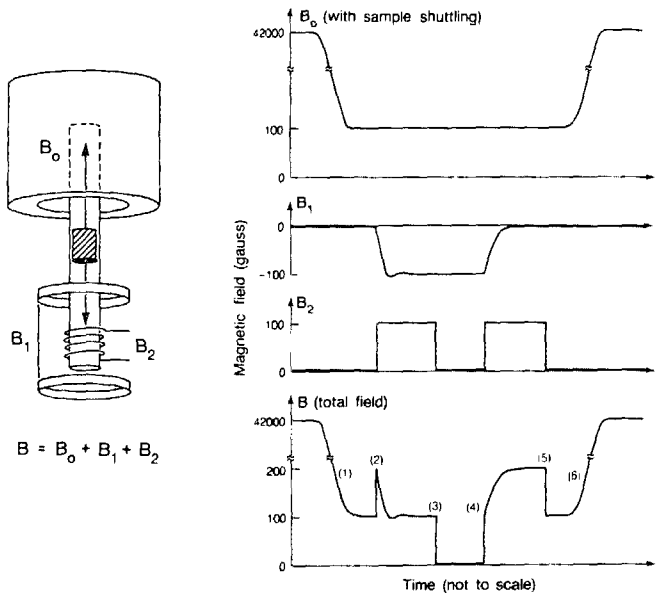

FIG. 3. Shown schematically at left, the arrangement of magnet coils and the sample shuttle system. B_0 represents a superconducting solenoid which is left on continuously. B_1 and B_2 are switchable room-temperature magnet coils. B_1 is designed to cancel the external fields including the fringe field of B_0. B_2 applies an intermediate field during the switching transients of B_1. At right, the sequence of sample shuttling and field switching which is used to form the field cycle. The labels (1) to (6) refer to the field cycle description in the text (Sec. I D). The sample shuttling (steps 1 and 6) occurs in about 150 ms each way; a period of 10 ms is allowed for the switching transitions of B_1; the small coil B_2 switches in about 300 ns.

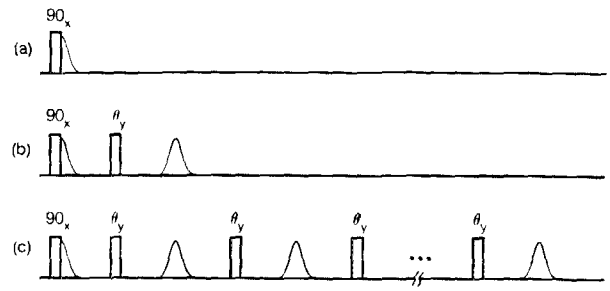

FIG. 4. Simple rf pulse sequences (rf magnetic field vs time) for the detection of nuclear magnetization at the end of each field cycle. The Gaussian curves represent the resulting free induction decays (fids) and spin echoes; optimally the signal would be recorded at the peaks of these curves. In (a) a single pulse produces an fid. The generation of a spin echo, shown in (b), offers the technical advantage that the signal appears well after the applied pulses and therefore can be measured more accurately. The optimal pulse angle θ depends on the nature of the spin system and the rf field strength, but is usually between 45° and 90°. If a series of spin echoes is formed as shown in (c), signal averaging over the entire echo train may yield a large increase in the signal-to-noise ratio.

sample is in zero field. (4) The zero-field interval ends when B_2 is turned back on. At that same time, B_1 is turned off. (5) After B_1 settles down, B_2 is turned off and only the fringe field remains. (6) The sample is then moved back into the main coil for the detection of the final magnetization.

Note that this field cycle includes two extra field transients [steps (2) and (5)] which are not essential from a theoretical perspective but which arise because of the different switching speeds of B_1 and B_2. When the intermediate field is much larger than the local fields, the extra field transients will have almost no effect. When this is not the case, it is expected that the extra field transients will cause some loss of signal. If this is a problem, it can be remedied by shaping the auxiliary coil current pulses so that their rise and fall at steps (2) and (5) matches the rise and fall of the shielding coil current pulses.

The high-field detection can be done by any method which results in a signal proportional to the nuclear magnetization. Figure 4(a) depicts the simplest detection sequence, which consists of the application of a 90° rf pulse to the sample, followed by the measurement of the initial amplitude of the free induction decay. In solids it is often preferable to record the signal amplitude after a spin-echo sequence[10] as shown in Fig. 4(b); this can eliminate the problems associated with the pulse recovery time of the probe and receiver. The spin echo pulse sequence may often be extended to generate a train of spin echoes[11] [Fig. 4(c)]. This can be used to improve the overall signal-to-noise ratio, since it allows rapid sampling of the magnetization as many as thousands of times for every field cycle.

II. THE INSTRUMENT

A. Basic NMR spectrometer

The design and construction of our zero-field apparatus is based on a preexisting homebuilt NMR spectrometer described in detail elsewhere.[12] Since any existing solid-state NMR spectrometer can be similarly adapted, we merely list the essential spectrometer characteristics:

The magnet (the main coil) is a persistent superconducting solenoid, contained in a Dewar vessel which has a room-temperature bore of 89 mm i. d. The field at the center is approximately 42 kG, corresponding to a proton Larmor frequency of 185 MHz, and is homogeneous to the extent of about 1 ppm over the sample volume used (approximately 6-mm-diam, 8-mm-long cylinders) without room-temperature shims.

The transmitter section is capable of producing spectrally pure rf pulses with rise and fall times of about 50 ns and with an amplitude precision better than 1 dB. Four phases, set 90° apart ($\pm 1°$), are available. The available pulse (peak) power is at least 1000 W at the Larmor frequencies of ^{2}D, ^{13}C, and ^{27}Al, and at least 600 W for protons. With our NMR probes, this is sufficient to obtain 90° pulse times of a few microseconds for each of the nuclei listed above.

The receiver section has an overall noise figure of 3 dB or better at the frequencies of interest. After the application of strong rf pulses, the receiver appears to fully recover in about 20 to 40 μs. This interval includes the ringdown time of the resonant probe circuit and the saturation recovery time of the receiver electronics. A phase sensitive superheterodyne detector is used to mix down the nuclear signal, yielding two audio frequency channels which correspond to two orthogonal phases of rf signal. The signal is then converted by two 10-bit analog-to-digital converters and stored in a digital memory system. The data can be converted and stored at any rate up to 1 point (two 10-bit numbers) per 3 μs.

The rf pulsing, data acquisition, magnet pulsing, and sample shuttling are all controlled by a homebuilt, high-speed multichannel programmable digital pulse generator,[13] which is capable of timing and producing sequences of many thousands of pulses, if necessary. The pulse lengths and delays may be set in increments of 100 ns.

B. Overview of the field cycling apparatus

The arrangement of the high-field and low-field magnets, shuttle system, and NMR probe is shown in Fig. 5. The Dewar vessel which contains the main coil is supported 75 cm above floor level. This allows easy access to the low-field apparatus placed below the Dewar, while permitting service of the NMR probe from above. All mechanical support structures in the low-field region are made of aluminum or brass except the coil forms, which are made of plastics. The rf coil of the NMR probe is of the "saddle shaped" configuration and is placed in the center of the main coil, where the field is found to be the most uniform. The low field coils are centered about the point on the axis of the main coil where its fringe field is 100 G.

C. Sample shuttle system

The sample is contained in a short plastic tube, as shown in Fig. 5(d). After the sample has been packed into the tube, a close-fitting cap is put on the open end, and the cap may then be held in place by a diametrical pin (not illustrated). All parts of the sample holder must be made out of an impact-resistant material. Nylon and kel-F work well in this regard.

The sample holder travels in a tube, the "shuttle tube," which runs between the high-field and low-field regions. The shuttle tube and its various attachments are illustrated in Figs. 5(b) and 5(c). At least at its ends, the shuttle tube itself must be electrically insulating, since time-varying magnetic fields are to be applied and eddy currents must be avoided. For satisfactory shuttling, the bore of the tube must be uniform. We have used ordinary thin-walled glass tubing, which seems suitable in both regards. The sample is driven up into the main coil by compressed air [about 6 psi (40 kPa) above atmospheric pressure] and down by a partial vacuum [about 10 psi (70 kPa) below atmospheric pressure] applied to the lower end of the shuttle tube. The upper end of the shuttle tube vents freely to the atmosphere.

At the upper end of the shuttle tube, upward motion of the sample is stopped by a thin-walled nylon or kel-F tube which extends down into the shuttle tube and is attached to the body of the NMR probe. The length of this stop is chosen so that the sample is accurately positioned within the rf coil during the detection sequence. The upper stop also serves in part to position the shuttle tube along the axis of the main coil.

At the lower end, the shuttle tube is attached to a glass-compatible T fitting (e.g. Cajon Co., Ultra-Torr model). The driving air or vacuum is applied to the central branch of that fitting. To stop the sample in the low-field region, a thin nylon rod extends up into the shuttle tube, and is attached to the lower branch of the T fitting by a screw which allows adjustment of the vertical position of the stop.

In the course of the shuttle cycle, a considerable mechanical impulse is delivered to each of the shuttle stops. It is therefore important that the NMR probe body and the T fitting, to which the stops are attached, are securely anchored to some steady supports.

The driving air and vacuum are switched through a commercial solenoid-actuated valve (e.g., Automatic Switch Company, Catalog No. 8320A89). The solenoid power is controlled by a simple semiconductor switching circuit, which takes a logic-level input signal. For most experiments, ac powered valves are suitable. Where spin-lattice relaxation times are short, reproducibility of the sample shuttling is important, and in such cases dc operated valves perform better as they tend to have more reproducible switching delay times.

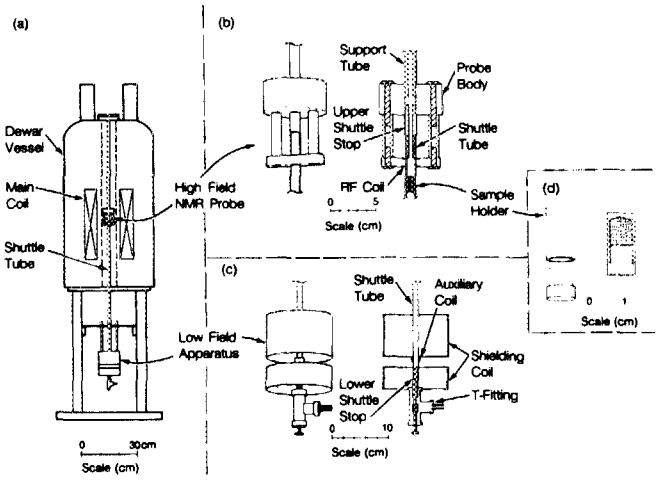

FIG. 5. In (a), the overview of the field cycling apparatus. Enlarged views of the high-field and low-field sections, and of the sample holder, appear in parts (b), (c), and (d), respectively.

D. Shielding coil system

In order to cancel the external field effectively, the shielding coil must match that field not only at a point but everywhere in the sample volume. That is to say that we must cancel the field and, to some degree, its gradients as well. The cancellation of field gradients, in general, is a difficult problem, but in this case a simplification results from the near symmetry of the external field. Since that field arises primarily from the main coil, which is a solenoid, the external field is very nearly cylindrically symmetric in the region of interest. This has the practical consequence that we can cancel the field quite effectively with a cylindrically symmetric coil aligned coaxially with the main coil.

In the low field region of our apparatus, the field and its gradients to third order are characterized by the following components:

$$B_z = 100.0 \text{ G},$$

$$\frac{\partial B_z}{\partial z} = 3.9 \text{ G/cm},$$

$$\frac{\partial^2 B_z}{\partial z^2} = 0.2 \text{ G/cm}^2,$$

$$\frac{\partial^3 B_z}{\partial z^3} = 0.01 \text{ G/cm}^3 \text{ (estimated)},$$

where the z axis is taken as parallel to the axis of the main coil. Our shielding coil system is designed to match the field and its first-order gradient, and to contribute nothing to the second-order gradient. If all works well, the residual field should then be due to the uncanceled second- and higher-order gradients of the external field, combined with any third- and higher-order gradients introduced by the shielding coil. In practice, with the coil geometry given below, the uncanceled second-order gradient accounts for most of the residual field; for samples of the size shown in Fig. 5(d), the residual field is about 25 mG at the ends of the sample, but somewhat better over most of the sample volume.

In order to minimize the higher-order gradients introduced by the shielding coil and the inductive coupling between the shielding coil and the auxiliary coil, one should make the length and diameter of the shielding coil as large as possible. Other factors, such as the coil resistance, the magnetic forces between the shielding coil and the main coil, and the possibility of transient currents induced in nearby metallic objects, argue for smaller shielding coils. The size of the coil described below was selected with these considerations in mind, although without any attempt at rigorous optimization. The arrangement of windings in the coil was chosen by numerical calculation with the aid of a programmable calculator. The geometry thus obtained yields the correct field and first-order gradient, and makes a negligible contribution to the second-order gradient. The coil was then wound in two uniform layers of 18 AWG (0.112 cm diameter) insulated copper wire on a rigid polymethacrylate tube to have the following dimensions [see Fig. 5(c)]: diameter: 11.43 cm, total length: 13.40 cm, length of lower segment: 4.00 cm, length of gap: 1.84 cm, length of upper segment: 7.56 cm, and pitch of coil windings: 0.127 cm. All of the windings are connected together in series. The field gradients are optimized about a point on the axis, within the gap and 0.54 cm below the upper coil segment.

The current through the shielding coil is controlled by a simple feedback network, as shown in Fig. 6. A logic-controlled switch allows shunting of the current control signal, and thus the current may be switched on and off. For some combinations of coil resistance and inductance, this circuit may oscillate continuously. The addition of an appropriate compensation network to the circuit can remedy such problems. The resistance of the magnet coil must be low enough that the steady-state coil voltage drop ($V = IR$) is less than about 20 V with the circuit shown.

When a single coil is used to cancel the external field, it is found that a relatively large residual field may arise from errors in the alignment and axial positioning of the shielding coil. To correct for such errors, we use a set of unswitched shim coils; shims to adjust B_x and B_y can correct for small alignment errors, and a symmetric first-order gradient shim

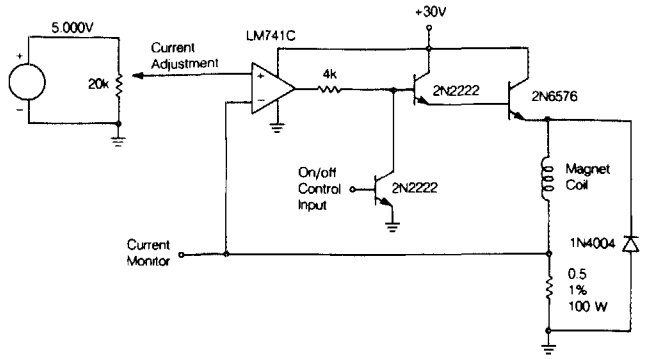

FIG. 6. Schematic diagram of the shielding coil power source. This circuit features a simple feedback network to regulate the current, with a shunting transistor added to permit switching of the output. They produce the on and off states, the control input current should be 0 and 10 mA, respectively.

can correct for errors in the axial position. These shims are placed around the outside of the shielding coil and are not shown in the figures.

The shielding coil system described here cancels only the static external field. No attempt has been made to cancel the time-varying (ac) fields, but this has not caused any serious problems for us since the ac field around our apparatus is relatively small ($\lesssim 5$ mG).

E. Auxiliary coil system

The auxiliary coil system must be rapidly switchable but need not produce a field of such spatial uniformity and field strength accuracy as the shielding coil system. Therefore the enclosed volume of the auxiliary coil may be relatively small and the coil current regulation relatively simple (i.e., without feedback). Both of these measures are used in this design to minimize the technical difficulty of rapid field switching.

The auxiliary coil is made in the form of a simple solenoid. It consists of 20 turns of 28 AWG (0.038 cm diameter) insulated copper wire wound uniformly in one layer on a nylon tube to make a coil of 1.2 cm diameter and 0.8 cm length.

The current through the auxiliary coil is switched in a standard fashion by the circuit shown in Fig. 7. One must use proper caution with this circuit since life-threatening voltages (about 200 V) are present. The use of the optical isolator is important mainly for reasons of safety. It allows the magnet coil to be at low voltages most of the time, and thereby reduces the risk of inadvertent electrical shock. Field-effect transistors were chosen as the switching elements because of their relatively high speed. In zero-field studies where the natural frequencies are low, switching speed is less critical and then bipolar transistors may be preferable for reasons of convenience or economy. For the current limiting and current sensing resistors (25 and 0.5 Ω, respectively in Fig. 7), ordinary wirewound resistors are to be avoided because of their relatively large inductances. However commercial "noninductive" wirewound resistors appear satisfactory.

The successful operation of the high-speed pulser circuit appears to depend strongly on the manner of construction.

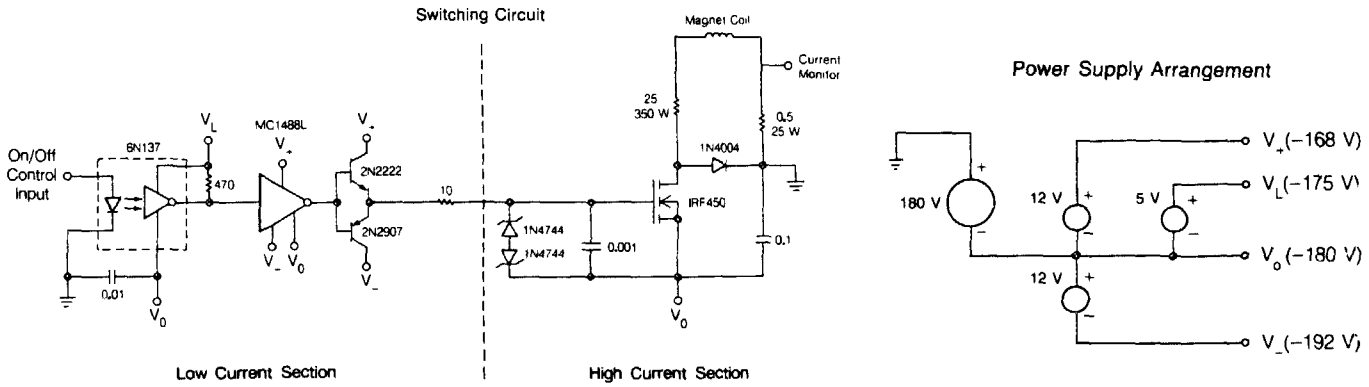

FIG. 7. Schematic diagram of the auxiliary coil power source. The low-power section consists of an optical isolator, to enhance personal safety, and a series of amplifiers. The high-power section is of a basic transistor switch design, with a flyback diode to limit the inductor voltage. Because of the high switching speed and large power involved, certain measures (see Sec. II E) are necessary to ensure electrical stability. To produce the on and off states, the control input current should be 8 and 0 mA, respectively. Resistances are expressed in ohms, and capacitances in microfarads.

Problems arise because the circuit has large amounts of gain and a small amount of feedback. The feedback is not part of the design, but arises from stray mutual inductances and capacitances between the high and low power sections of the circuit. The distinction between these two parts of the circuit is indicated in Fig. 7. If there is too much feedback the circuit becomes unstable and continuous rf oscillations result which may damage the power transistor. As a remedy, it appears best to isolate these two sections by spatially separating them, avoiding (when possible) shared panels or cables which might transmit unwanted feedback signals, and avoiding unnecessarily long wires or large loops within each separate section.

The stability and transient response of this circuit are further enhanced by the liberal use of small capacitors (0.001 to 0.1 μF) near sensitive circuit components. The placement of these capacitors rather close to associated circuit elements is important, in order to minimize the effects of lead inductances. Three such capacitors are shown in Fig. 7. There are additionally (not shown in Fig. 7) 0.1 μF capacitors in parallel with the 5-V supply and each of the 12-V supplies. These capacitors are required to maintain nearly constant supply voltages in the face of rapidly changing supply currents. They should be placed near points of current demand.

III. OPERATION

A. Setup

In addition to the equipment mentioned in Sec. II, it is also necessary to have an instrument for measuring the magnetic field in the low-field region. This is especially important when first setting up the apparatus. In routine use, a Hall effect gaussmeter (e.g., F. W. Bell Inc., model 811A gaussmeter) is recommended. In the small and inhomogeneous fields encountered, Hall effect instruments are probably more useful than instruments which employ NMR or ferromagnetic effects for magnetic field detection.

Before construction of the shielding coil and the low-field support structures, it is necessary to measure the field and characterize the field gradients in the low-field region. Later, when the coil and its supports are in place, the coil current and alignment must be set. This is most readily done if one can measure the magnitude and direction of the residual field $\mathbf{B}_0 + \mathbf{B}_1$. A residual field oriented along the axis of the coil indicates an error in the shielding coil current; a residual field perpendicular to the coil axis indicates an error in the orientation of the shielding coil; a residual field gradient which is first order and axially symmetric suggests that an error exists in the axial position of the shielding coil relative to the main coil.

In the setup procedure and more generally when operating the apparatus, some care must be taken to avoid operating the shielding and auxiliary coils with an excessive "duty factor" (fraction of time when current is on). At duty factors of 0.1 or larger, the shielding coil power source may suffer a slight and temporary loss of accuracy due to heating of the current sensing resistor (from the coil to ground in Fig. 6). At yet higher duty factors, the current limiting resistor in the auxiliary coil power source may burn out, and permanent damage to the coils or their forms may result from resistive heating in the coil windings.

Once the setup adjustments are finished, the residual field can be characterized by means of zero-field NMR experiments. This is sometimes helpful but not usually necessary. Solid samples with relatively weak local nuclear interactions show a slight spreading or splitting of the spectral lines when there is a moderate residual field. Zero-field spectra of liquid samples, with J couplings or without, are more sensitively affected by very slight residual fields as the natural linewidths are smaller. One may of course use such measurements to make further adjustments and refinements of the residual field.

B. Routine operation

As mentioned in the Introduction, many field cycles must be performed in order to measure the zero-field magne-

tization decay curve, since each field cycle provides information about only one point on that curve. Each field cycle should begin with a high-field polarization period at least as long as T_1 so that the initial magnetization is large. The values of the zero-field interval t_1 are best chosen as regularly incremented times starting with $t_1 = 0$. This makes the computation of the Fourier transform convenient. The time increment Δt_1 should be short enough that there is no aliasing of the signal, that is $\Delta t_1 < \pi/\omega_{\max}$ in keeping with the sampling theorem. An approximate estimate of this time increment may be derived from the high-field spectrum, since generally the zero-field frequencies are on the order of the width of the high-field powder pattern.

The technique described in Sec. I demands that the spin-lattice relaxation time constant (T_1) of the nuclear species of interest is not much shorter than the minimum time required to execute the field cycle (essentially the round-trip shuttle time, about 300 ms). If the T_1 is less than that, it may be difficult or impossible to obtain the zero-field spectrum since little evolved magnetization will survive to the end of the field cycle. This is the constraint given in expression (1). Thus, before attempting this zero-field technique with any sample, it is advisable to determine the suitability of the T_1. The high field T_1 can be conveniently measured by, for example, saturating the nuclear spins and monitoring their recovery towards the equilibrium polarization. With some samples the zero-field signal vanishes or is greatly reduced during the field cycle, even though the high field T_1 is sufficiently long. In some cases that is merely because the spin-lattice relaxation is too rapid in the lower fields. In other cases the signal may be lost through heteronuclear spin–spin relaxation processes, which can be very rapid at certain intermediate field strengths.[14]

For many samples of interest, the restrictions on T_1 imposed by the experimental technique of Sec. I are a serious drawback. Alternative instrumentation techniques may reduce or remove such problems. For example, the method proposed below in Sec. V D may be feasible without the slow field transitions which at present limit the technique to samples with moderately long T_1's.

IV. SAMPLE DATA

In this section, we begin with a comparison of high-field and zero-field NMR techniques as applied to the protons in lithium sulfate hydrate, $Li_2SO_4 \cdot H_2O$. In this compound, the protons are grouped closely in pairs (the H_2O molecules), so one might expect them to behave approximately as two-spin dipolar-coupled systems. The proton T_1 is about 1 s, and the experiments presented here were done with a cycle time of approximately 3 s.

Figure 8(a) shows the high-field free induction decay (fid) of the protons in a polycrystalline sample of $Li_2SO_4 \cdot H_2O$, along with its Fourier transform which is the ordinary NMR spectrum. In this case, the pulse recovery time of our probe ($\sim 40\,\mu$s) is somewhat longer than the fid, so it is necessary to use a dipolar echo sequence [90_x, τ, 90_y, τ, acquire; see Fig. 4(b)], with an echo delay $\tau = 40\,\mu$s. The acquisition consisted of recording the signal

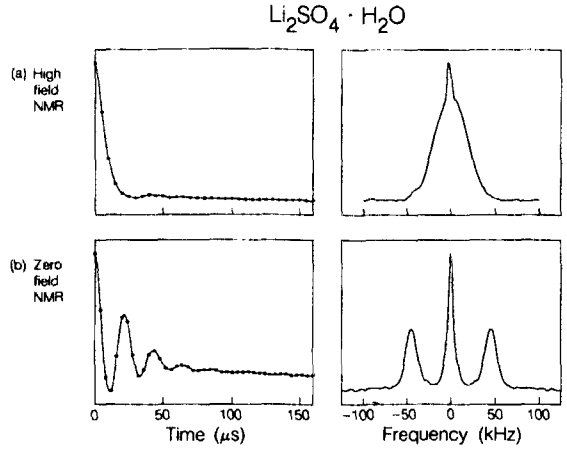

FIG. 8. Proton NMR signals of polycrystalline lithium sulfate hydrate. In (a) at left, the high-field signal as obtained in the time domain. The dots show the actual data; the curve is for visual clarity. At right, its Fourier transform, which is the high-field spectrum. The data shown in (a) are the average of 200 scans, measured in about ten minutes. Part (b) shows the zero-field time-domain signal and the corresponding spectrum. The improved resolution results mainly from the removal of the frequency spreading which is unavoidable in high field. The data in (b) are the average of 147 scans of 64 field cycles each (however the time-domain plot shows only the first 41 points), acquired in approximately 8 h. The high-field detection was performed by a simple spin echo sequence. With more efficient detection schemes (e.g., a multiple echo sequence) the acquisition time can be substantially reduced.

at regular 5-μs intervals, affording a spectral bandwidth of 200 kHz. For isolated pairs of dipolar-coupled spin-1/2 nuclei, the dipolar echo sequence accurately gives the NMR spectrum. Regardless of that, the high-field powder spectrum reveals no distinct spectral features, and is not very useful.

The zero-field magnetization decay and the corresponding spectrum are shown in Fig. 8(b). The dipolar echo sequence was employed for the detection here also, but in this case only a single point was sampled at the peak of each echo. The increment in t_1 was 4 μs, corresponding to a bandwidth of 250 kHz. The simple spectral pattern of three lines is characteristic of homonuclear spin-1/2 pairs. The line spacing $\Delta\omega$ is related to the internuclear distance r as

$$\Delta\omega = 3\gamma^2 \hbar/2r^3 ,$$

and using the experimental peak frequencies we calculate a nearest-neighbor interproton distance of 1.58 Å. This agrees closely with work on single crystals of $Li_2SO_4 \cdot H_2O$, employing high field NMR[15] and neutron diffraction[16] techniques. The weaker dipolar couplings, those between non-nearest-neighbor protons and those between protons and lithium nuclei, determine the line shapes and linewidths. In certain cases[17] such extra couplings introduce additional splittings in the spectrum which may be interpreted to yield additional distances and angles.

For nuclei with spin $I > 1$, quadrupolar interactions are present and are usually much larger than the dipolar interactions. As a result, their zero-field spectra tend to be more informative about the bonding and symmetry about individual nuclear sites. The quadrupolar frequencies are indicative

of the chemical nature of the nuclei, in much the same way as chemical shifts are in high-field NMR. Figure 9 shows the zero-field deuterium spectrum of a polycrystalline sample of 1,8-dimethylnaphthalene-d_{12}. Components of the signal appear in three distinct spectral bands. Around 130 kHz there are a number of peaks, which are assignable to the ^{2}D nuclei at the aromatic ring sites. The spectral structure in this region arises in part from the asymmetry of the electric field gradient around each site, and in part from the chemical inequivalence of the various aromatic sites. The signal near 35 kHz is associated with the methyl groups. Aliphatic deuteron signals usually appear about 110 kHz; that the signal appears at only 35 kHz is a consequence of the rapid rotational motions of the methyl groups, which partially average the electric field gradients at those deuteron sites. The splittings in that band arise from dipolar couplings between the methyl deuterons. The lines in the range of 0 to 10 kHz are assignable to either methyl or aromatic sites. The frequencies observed in this range correspond to splittings within the higher frequency bands.

For this experiment an intermediate field of 300 G was used. This required the construction of new shielding and auxiliary coils adapted to the higher field. The experiment was performed with a cycle time of 10 s, which is several times longer than the methyl T_1's, and comparable to the aromatic T_1's. A zero-field time increment of 3 μs was used. The high field detection was accomplished by a multiple echo sequence of 1024 echoes.

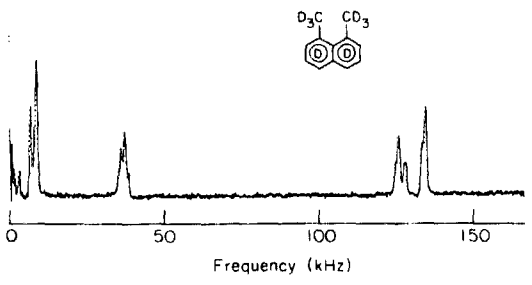

FIG. 9. Zero-field deuterium spectrum of polycrystalline 1,8-dimethylnaphthalene-d_{12}. The group of peaks about 130 kHz represents signal from the ^{2}D nuclei at sites on the aromatic rings. The signal near 35 kHz arises from the deuterons at the methyl sites, where the rapid rotational motions cause a decrease in the effective quadrupolar interaction. This spectrum is the result of four scans of 1001 field cycles each, measured with a total acquisition time of about 11 h.

V. VARIATIONS AND IMPROVEMENTS

A. Pulsed fields

For many quadrupolar spin systems, the field cycle of Fig. 2 may be difficult to execute because the required intermediate field and switching speed are both high and therefore the electrical power requirements (see Sec. I C) are excessive. Other field cycling schemes may then be technically more feasible. Figure 10 shows one such scheme. Here the preparation and detection intervals include adiabatic (i.e., $1/\omega_{max} \ll \tau_s \ll T_1$) field shifts to and from zero field. During the zero-field interval, coherent evolution of the spin order is

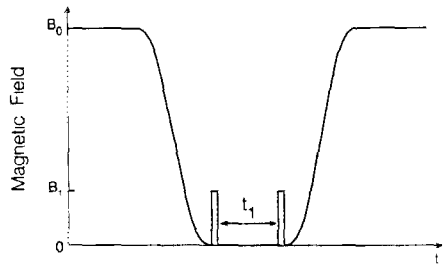

FIG. 10. An alternative field cycling scheme. Here the transitions from high field to zero field and back are done entirely adiabatically, and zero-field evolution is initiated and terminated by brief field pulses. Compared to the scheme shown in Fig. 2, this scheme can be technically easier when the nature of the spin system calls for a very large intermediate field.

initiated by the application of a short intense field pulse. Strong pulses, either dc or rf, transform the stationary spin order created by the adiabatic demagnetization into coherences, which evolve for a time t_1. Then the coherences are transformed back into stationary states by a second pulse. Following adiabatic remagnetization, the evolved signal can be detected in high field. As before, the signal is measured for regularly incremented values of t_1 and Fourier transformed to yield the zero-field spectrum.

In comparison to the sudden switching scheme of Fig. 2, this pulsed field cycling scheme suffers from the disadvantage that its results are more difficult to analyze theoretically. However pulsed field cycling appears technically easier since the demands placed on the electronics are of relatively short duration. For systems of quadrupolar nuclei near spin-1/2 nuclei, the pulsed scheme allows indirect detection of the quadrupolar signal through the high-field signal of the spin-1/2 nuclei. This indirect detection is well known in frequency-domain field cycling work.[2,4] Owing to the large magnetic moment of the proton and the relatively small spectral width of its high-field NMR signal, when indirect detection via protons can be performed, a significant gain in sensitivity may be realized. The various technical and experimental advantages of pulsed NQR schemes are discussed in more detail, with illustrative experimental results, in recent articles.[8,9]

B. Ferromagnetic shielding

In the method of Sec. I D, a coil is used to shield the sample from external fields. This shielding can be done as well, and perhaps better, by an enclosure made of ferromagnetic materials. With such an enclosure, the ferromagnetic walls tend to gather the external magnetic flux, thus diverting it from the enclosed region.[18] Fields on the order of milligauss are readily obtained in this fashion. We have used ferromagnetic shielding successfully in a study of J couplings in liquids in zero field, and other workers have used the idea for pulsed zero-field NQR experiments.[9] The possible advantages of ferromagnetic shielding derive in part from the fact that, within a certain range of fields, the ferromagnetism responds closely to changes in the external field. Thus the external field and its gradients do not have to be very accura-

tely known beforehand, and the shield automatically cancels time-varying fields as well as static fields. This may make the construction and setup procedures much easier, and would increase the reliability and stability of the apparatus.

C. Switchable main coil

Instead of moving the sample between the center and the fringe of the main coil in order to remove and restore the high field, one may obtain the same effect by keeping the sample stationary and varying the current through the main coil. Such a technique is often used for field-dependent T_1 studies.[6] The switching of very large magnetic fields at moderate speeds ($\sim$400 kG in $\sim$5 ms) has been applied to other sorts of magnetic studies.[19] This kind of magnet switching may allow more rapid field cycling than mechanical sample shuttling and should be important where spin-lattice relaxation times are short. It may prove useful in studies of single crystals, liquid crystals, or otherwise fragile samples, where it is important to avoid pulverizing, stirring, or stressing the sample. It may also be useful in variable-temperature zero-field studies, where it is best to keep the sample localized in a thermally insulated region near a heating or cooling device. Disadvantages of this scheme arise from the mechanical strain of the main coil due to the time-varying magnetic forces and resistive heating. These effects tend to limit the constancy (both short term and long term) and homogeneity of the high field, which in turn degrade the efficiency and accuracy of the detection sequence.

D. Direct detection

In most NMR experiments, the signal is picked up by a magnet coil, in accordance with Faraday's Law:

$$|\mathscr{E}| \sim \frac{d\Phi}{dt} \sim \omega M_z ,$$

where $\mathscr{E}$ is the electromotive force associated with the magnetic flux Φ, ω is the characteristic frequency and M_z is the magnetization to be detected. Since the measured voltage or current is usually proportional to $|\mathscr{E}|$, the measured signal amplitude is proportional to the signal frequency. As mentioned in the Introduction, this frequency dependence contributes to the sensitivity problem of observing NMR directly in zero field. There are alternative detection devices which do not suffer from this strong frequency dependence. The most promising alternatives at this time involve the use of superconducting quantum interference devices (SQUIDs). These may be used as magnetic flux detectors (the resulting electrical signal is proportional to Φ, not $d\Phi/dt$) and are known to be effective for monitoring nuclear magnetizations at low frequencies.[20]

In zero-field NMR studies using SQUID detectors, the zero-field magnetization decay might be measured directly and in its entirety, rather than indirectly and pointwise. An appropriate field cycle includes a sudden field shift, going from some preparation field level to zero, with free evolution and detection occurring simultaneously in zero field. Only a single field cycle, rather than a series of many cycles, obtains the entire magnetization decay curve. Possible advantages of this scheme in comparison to that of Sec. I include that it may yield more rapid measurements in some cases, and it may allow zero-field experiments to be done with a simpler and smaller apparatus. The field cycles used for direct detection schemes may of course include a simple or a two-step field transition, in the manner of Fig. 1 or 2, respectively. The former may be preferable for reasons of simplicity, while the latter offers higher sensitivity. Alternatively the application of a short dc or rf pulse to a demagnetized sample can be used to produce a transient magnetization for direct detection experiments.

ACKNOWLEDGMENTS

We thank Donald Wilkinson and David Gee for advice and helpful discussions during the design of the high-speed (auxiliary coil) pulser electronics. During the course of this work, one of us (D. B. Z.) was supported by a National Science Foundation Graduate Fellowship. This work was supported by the Director, Office of Energy Research, Office of Basic Energy Sciences, Materials Sciences Division of the U. S. Department of Energy, and the Director's Program Development Funds of the Lawrence Berkeley Laboratory, under Contract DE-AC03-76SF00098.

[a] Current address: Isotope Division, Weizmann Institute of Science, Rehovot 76100, Israel.
[b] Current address: Department of Chemistry, Yale University, New Haven, CT 06511.

[1] (a) N. Bloembergen and T. J. Rowland, Acta Metall. **1**, 731 (1953); (b) G. E. Pake, J. Chem. Phys. **16**, 327 (1948).
[2] Reviews: (a) R. Blinc, Adv. Nuc. Quad. Reson. **2**, 71 (1975); (b) D. T. Edmonds, Phys. Rep. **C29**, 235 (1977); (c) D. T. Edmonds, Int. Rev. Phys. Chem. **2**, 103 (1982).
[3] (a) N. F. Ramsey and R. V. Pound, Phys. Rev. **81**, 278 (1951); (b) A. G. Anderson, Phys. Rev. **115**, 863 (1959); (c) A. G. Anderson, Phys. Rev. **125**, 1517 (1962).
[4] (a) A. G. Redfield, Phys. Rev. **130**, 589 (1963); (b) R. E. Slusher and E. L. Hahn, Phys. Rev. **166**, 332 (1968); (c) J. Koo and Y.-N. Hsieh, Chem. Phys. Lett. **9**, 238 (1971); (d) Y. Hsieh, J. C. Koo, and E. L. Hahn, Chem. Phys. Lett. **13**, 563 (1972); (e) R. Blinc, M. Mali, R. Osredkar, A. Prelesnik, J. Seliger, and I. Zupancic, J. Chem. Phys. **57**, 5087 (1972); (f) O. Lumpkin, J. Chem. Phys. **62**, 3281 (1975); (g) T. Maruizumi, Y. Hiyama, N. Watanabe, and E. Niki, Bull. Chem. Soc. Jpn. **51**, 978 (1978); (h) L. S. Batchelder, J. Clymer, and J. L. Ragle, J. Chem. Phys. **74**, 4791 (1981); (i) C. R. Brett and D. T. Edmonds, J. Magn. Reson. **49**, 304 (1982); (j) T. L. Brown, L. G. Butler, D. Y. Curtin, Y. Hiyama, I. C. Paul, and R. B. Wilson, J. Am. Chem. Soc. **104**, 1172 (1982); (k) M. Suhara and J. A. S. Smith, J. Magn. Reson. **50**, 237 (1982); (l) I. J. F. Poplett, J. Magn. Reson. **50**, 382 (1982).
[5] (a) R. L. Strombotne and E. L. Hahn, Phys. Rev. **A133**, 1616 (1964); (b) M. Packard and R. Varian, Phys. Rev. **93**, 941 (1954).
[6] (a) A. G. Redfield, W. Fite, and H. E. Bleich, Rev. Sci. Instrum. **39**, 710 (1968); (b) K. Hallenga and S. H. Koenig, Biochemistry **15**, 4255 (1975); (c) R. D. Brown III, C. F. Brewer, and S. H. Koenig, Biochemistry **16**, 3883 (1977); (d) M. Stohrer and F. Noack, J. Chem. Phys. **67**, 3729 (1977); (e) G. Nagel, W. Woelfel, and F. Noack, Isr. J. Chem. **23**, 380 (1983); (f) R. G. Bryant and M. Jarvis, J. Phys. Chem. **88**, 1323 (1984); (g) C. F. Polnaszek and R. G. Bryant, J. Chem. Phys. **81**, 4308 (1984); (h) S. H. Koenig and R. D. Brown, III, J. Magn. Reson. **61**, 426 (1985).
[7] (a) D. P. Weitekamp, A. Bielecki, D. Zax, K. Zilm, and A. Pines, Phys. Rev. Lett. **50**, 1807 (1983); (b) A. Bielecki, J. B. Murdoch, D. P. Weitekamp, D. B. Zax, K. W. Zilm, H. Zimmerman, and A. Pines, J. Chem.

Phys. **80**, 2232 (1984); (c) D. B. Zax, A. Bielecki, K. W. Zilm, and A. Pines, Chem. Phys. Lett. **106**, 550 (1984); (d) D. B. Zax, A. Bielecki, A. Pines, and S. W. Sinton, Nature **312**, 351 (1984); (e) D. B. Zax, A. Bielecki, D. P. Weitekamp, K. W. Zilm, and A. Pines, J. Chem. Phys. **83**, 4877 (1985).

[8] J. M. Millar, A. M. Thayer, A. Bielecki, D. B. Zax, and A. Pines, J. Chem. Phys. **83**, 934 (1985).

[9] R. Kreis, D. Suter, and R. R. Ernst, Chem. Phys. Lett. **118**, 120 (1985).

[10] (a) E. L. Hahn, Phys. Rev. **80**, 580 (1950); (b) H. Y. Carr and E. M. Purcell, Phys. Rev. **94**, 630 (1954); (c) I. Solomon, Phys. Rev. **110**, 61 (1958); (d) P. Mansfield, Phys. Rev. **A137**, 961 (1965); (e) I. D. Weisman and L. H. Bennett, Phys. Rev. **181**, 1341 (1969).

[11] (a) E. D. Ostroff and J. S. Waugh, Phys. Rev. Lett. **16**, 1097 (1966); (b) W.-K. Rhim, D. P. Burum, and D. D. Elleman, Phys. Rev. Lett. **37**, 1764 (1976); (c) D. Suwelack and J. S. Waugh, Phys. Rev. B **22**, 5110 (1980); (d) M. M. Maricq, Phys. Rev. B **25**, 6622 (1982).

[12] S. W. Sinton, Ph.D. thesis, University of California, Berkeley (1981).

[13] G. P. Drobny, Ph.D. thesis, University of California, Berkeley (1982).

[14] M. Goldman, C. R. Acad. Sci. **246**, 1058 (1958).

[15] B. Pedersen and D. F. Holcomb, J. Chem. Phys. **38**, 61 (1963).

[16] H. G. Smith, S. W. Peterson, and H. A. Levy, J. Chem. Phys. **48**, 5561 (1968).

[17] D. B. Zax, A. Bielecki, M. A. Kulzick, E. L. Muetterties, and A. Pines, J. Phys. Chem. (to be published).

[18] J. D. Jackson, *Classical Electrodynamics*, 2nd ed. (Wiley, New York, 1975), pp. 199–201.

[19] (a) V. I. Ozhogin, K. G. Gurtovoj, and A. S. Lagutin, in *High Field Magnetism*, edited by M. Date (North-Holland, Amsterdam, 1982); (b) A. Yamagishi and M. Date, in *High Field Magnetism*, edited by M. Date (North Holland, Amsterdam, 1982); (c) A. P. J. van Deursen and A. R. de Vroomen, J. Phys. E **17**, 155 (1984).

[20] (a) G. J. Ehnholm, J. P. Ekstrom, M. T. Loponen, and J. K. Soini, Cryogenics **19**, 673 (1979); (b) G. J. Ehnholm, J. P. Ekstrom, J. F. Jacquinot, M. T. Loponen, O. V. Lounasmaa, and J. K. Soini, J. Low Temp. Phys. **39**, 417 (1980); (c) C. Hilbert, J. C. Clarke, T. Sleator, and E. L. Hahn (unpublished).